Modelling of a linear PM machine including magnetic saturation and end effects: maximum force to current ratio

H. Polinder, J.G. Slootweg, M.J. Hoeijmakers
Delft University of Technology
Mekelweg 4, 2628 CD Delft
The Netherlands

J.C. Compter
Eindhoven University of Technology
Den Dolech 2, 5600 MB Eindhoven
The Netherlands

***Abstract* – The use of linear permanent-magnet (PM) actuators increases in a wide variety of applications because of their high force density, robustness and accuracy. These linear PM motors are often heavily loaded during short intervals of high acceleration, so that magnetic saturation occurs. This paper models saturation and end effects in linear PM motors using magnetic circuit models. The saturating parts of the magnetic circuit are modelled as non-linear reluctances. Magnetomotive forces represent the currents and the magnets. This paper shows that when saturated, a negative d-axis current increases the force developed by the motor. Although the increase is not large, it is nevertheless useful, because a negative d-axis current also results in a decrease in the amplifier rating. Further, the trajectory for the maximum force to current ratio is derived. The correlation between the calculated and the measured force justifies the model.**

I. INTRODUCTION

A trend to increase the use of linear electro mechanic actuators can be observed in a wide range of applications, from aeroplanes (fly by wire) to factory automation [1,2]. Important advantages of linear electro mechanic actuators are that they are clean, robust, and efficient and that they can be fed from simple copper wires. Further, direct-drive actuators can have a high positioning and speed accuracy because no mechanic transmission is necessary.

For demanding applications, the linear motors are mostly of the permanent magnet type, because compared to other linear electric motors, they have a high force density, a high efficiency and a relatively simple control.

This paper deals with a linear permanent-magnet (PM) motor applied for horizontal micrometre positioning in wafer steppers and component placing machines. To control such a system accurately and with a high performance, classical feed-back control systems are not suitable because they make forces based on position errors, which implies the presence of these position errors. Instead, feed-back control should be combined with feed-forward control [3], where all available information about the system is used to prevent errors. For example, information about moving masses and the desired position and speed profiles is used to calculate the force necessary to obtain the desired position and speed profile. In this case, the feed-back controller only has to eliminate errors due to unpredictable phenomena. Therefore, a good feed-forward control must be able to predict the force developed by the motor.

When the currents are low, the motor does not saturate and the force is well-predictable linearly proportional to the current. However, during short intervals of heavy acceleration, the currents are so high that the magnetic circuit saturates, and the force is not easily predictable, which complicates the control.

Therefore, the goal of this paper is to model the motor in such a way that the force generated by the linear motor can be predicted as a function of the current and the position. This model is used to maximize the force to current ratio. To investigate end effects, two modes are compared, one neglecting, and the other incorporating end effects.

For interior PM motors, using negative d-axis currents to maximize the force to current ratio is common practice [4-9]. In these machines, a negative d-axis current results in an additional force because of the reluctance effect. A maximum thrust per amp trajectory for linear interior permanent-magnet motors is derived in [4]. Saturation is included for rotating motors in [5] and for linear motors in [6].

However, [5,8,9] state that maximum torque (or force) to current control in motors with surface-mounted permanent magnets is achieved when the d-axis current is kept zero, or in other words when the angle between the no-load voltage and the current is kept zero. This statement is true for motors which are not heavily loaded so that saturation is negligible. However, this paper investigates the effect of a negative d-axis current on the force when saturation occurs and concludes differently.

Besides, negative d-axis currents are used to extend the speed range of PM machines, which is mostly referred to as flux weakening [4,6-9]. This is mostly applied in PM machines with interior magnets; in machines with surface-mounted magnets, the increase in the speed range is limited [9]. However, in a motor with surface magnets, adding a negative d-axis current as well results in a reduction of the volt-ampere rating of the amplifier or the inverter [8,9]. This effect is useful in our application.

Furthermore, negative d-axis currents are used to minimize the sum of the core losses and the copper losses in PM machines [10, 11]. However, in linear motors, the core losses mostly are small compared to the copper losses because of the relatively low speeds, so that this effect is not important.

It is possible to calculate the motor force using Finite Element Methods [12]. Here, we use a magnetic circuit model, like in [13, 14], because with such a model, trends can be observed faster and because it can be used easier in optimization programs, for example, to search for maximum

0-7803-7817-2/03/$17.00 ©2003 IEEE

force to current ratio trajectories. Magnetomotive forces represent the currents and the magnets. The saturating parts of the magnetic circuit are modelled as non-linear reluctances.

This paper first characterizes the investigated motor. Then, it describes the magnetic circuit modelling of the motor and gives expressions for voltages and forces. Subsequently, calculated and measured results are given and compared to validate the model. Finally, conclusions are drawn.

II. Motor Description

Fig. 1 depicts a photo of the linear permanent-magnet motor; Fig. 3 depicts a schematic section. Table I lists some important dimensions. The magnets are on the bottom plate. The translator has a fractional pitch winding with the following advantages.

- The winding consists of coils around a tooth with simple short end windings that can be wound outside the motor.
- The orthocyclic method of coil winding described by Lenders [15] can be used, which results in a high copper filling factor of the slots and a good heath transfer from the coils to the back iron.
- The translator yoke and the back-iron behind the magnets can be thin compared to a machines with larger pole-pitches and full-pitch windings [1].

In Fig. 3, a phase consist of four series-connected coils. When the translator moves over the magnets, a three-phase voltage is induced in the star-connected phases. As shown in Fig. 2, this voltage is almost sinusoidal due to the chosen magnet width and the skewing of the magnets. Fig. 2 also gives the no-load flux linkages, obtained from integrating the no-load voltages.

A position sensor detects the position of the translator. Based on this position information, a power amplifier generates a three-phase sinusoidal current.

TABLE I
PM Motor Dimensions.

description	symbol	size
pole pitch	τ_p	12 mm
magnet thickness	h_m	4 mm
magnet width	b_m	8 mm
magnet length	l_m	60 mm

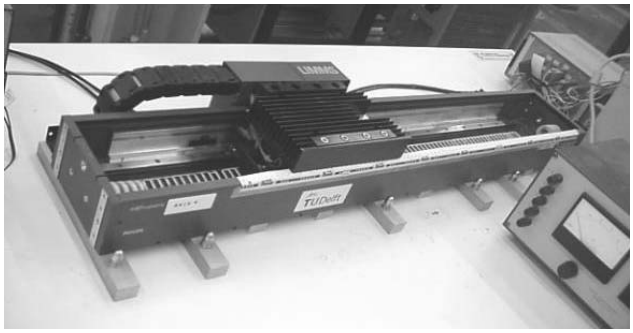

Fig. 1. Photo of the linear PM machine with magnets on a bottom plate and a translator with coils.

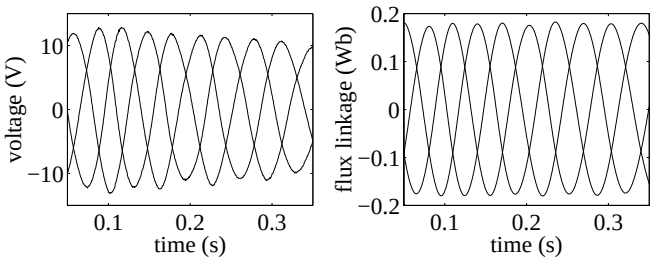

Fig. 2. Measured no-load phase voltages and flux linkages; the speed is not constant.

III. Magnetic Circuit Modelling

A. Equivalent magnetic circuit model

In this section, two magnetic circuit models of the linear motor are derived. In these models, the fluxes in the teeth are the most important variables, because these fluxes link with the translator coils and are used for the calculation of the force.

Fig. 4 depicts the first magnetic circuit model of the motor. In this model, it is assumed that only the translator teeth (around which the coils are wound) and the translator yoke saturate. Because the flux density in the back-iron is lower, the reluctance of the back-iron is neglected.

In order to obtain the second, further simplified model of Fig. 5, the yoke reluctance, end effects and end teeth are neglected in such a way that the machine is modelled as if it were infinitely long or as if it were a cylindrical motor. Also the reluctance of the translator yoke is neglected. In this case, it is sufficient to consider three translator teeth.

B. Reluctance values

A general expression for the value of a reluctance is

$$R_m = \frac{l_c H}{A_c B} \tag{1}$$

where

H is the magnetic field intensity in the circuit,
B is the magnetic flux density in the circuit,
l_c is the length of the magnetic circuit, and
A_c is the cross-section of the magnetic circuit.

With this equation, the air-gap reluctance R_{mg} (the reluctance between a tooth and the back iron) can be expressed as

$$R_{mg} = \frac{k_C(g + h_m/\mu_{rm})}{\mu_0 l_s (b_t + b_s)} \tag{2}$$

where

k_C is the Carter factor [16],
g is the air-gap length,
h_m is the magnet length in the magnetization direction,
μ_{rm} is the recoil permeability of the magnets,
μ_0 is the magnetic permeability in vacuum,
b_s is the slot width,
b_t is the tooth width, and

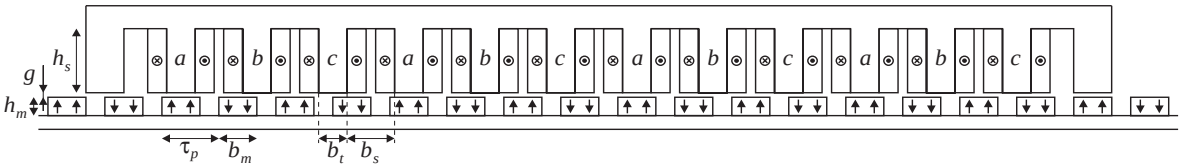

Fig. 3. Section of the linear permanent-magnet motor with some dimensions.

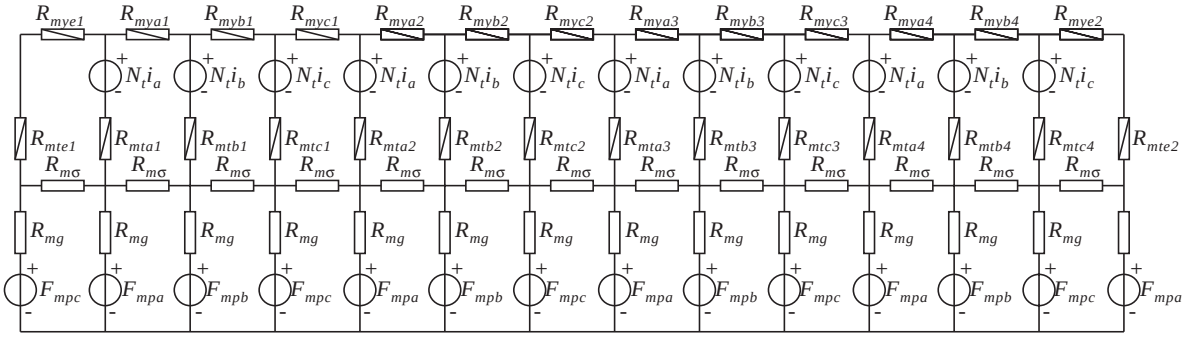

Fig. 4. Magnetic circuit model of the linear permanent-magnet motor including end effects.

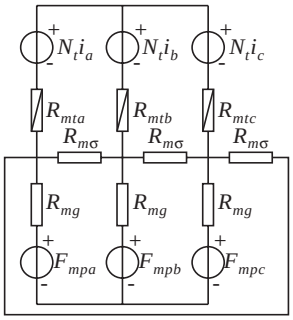

Fig. 5. Simplified magnetic circuit model of the linear PM motor neglecting end effects.

l_s is the stack length, the length in the direction perpendicular to the plane of the drawing in Fig. 3.

In this equation, the width of the flux path is taken the tooth pitch (tooth width plus slot width) because the flux crosses the air gap over the whole tooth pitch due to flux fringing. The average path length of the flux path is the air gap length multiplied by the Carter factor, which takes into account that the fringing flux follows a longer path [16].

The slot leakage reluctance $R_{m\sigma}$ is calculated as

$$R_{m\sigma} = \frac{2b_s}{\mu_0 h_s l_s} \tag{3}$$

where h_s is the slot height.

The factor 2 in this equation takes into account that the slot leakage flux density increases linearly from zero close to the yoke to a maximum close to the air gap.

The starting point for the determination of the tooth reluctance is the measured the *BH*-curve of the magnetic material [17] and depicted in Fig. 6. This *BH*-curve is approximated with a function also depicted in Fig. 6:

$$H = 150B + 15B^{11} \tag{4}$$

If we use this expression in the general expression for a reluctance, we obtain the tooth reluctance R_{mt} as

$$R_{mt} = \frac{2h_s}{3b_t l_s}(150 + 15B_t^{10}) \tag{5}$$

In this equation, the circuit surface is the cross-section of a tooth, and the length is taken as two third of the tooth height, because leakage flux enters the tooth over the whole height, so that the lower part does not saturate.

In the same way, we obtain the yoke reluctance R_{my} as

$$R_{my} = \frac{b_s}{h_y l_s}(150 + 15B_t^{10}) \tag{6}$$

where h_y is the translator yoke height.

C. Magnetomotive forces

The magnetomotive force of a translator current equals the phase current multiplied by the number of turns of the coil around a translator tooth N_t.

The magnets also cause a flux in the translator teeth. This flux is determined from the measured no-load voltage of Fig. 2.

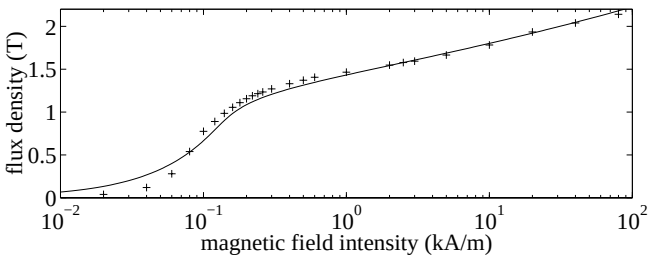

Fig. 6. Measured BH-curve of the magnetic material (+) and the approximation used in the calculations.

The flux varies sinusoidally, as can be concluded from the sinusoidal form of the no-load voltages. Hence, the fluxes in the translator teeth due to the magnets are given by

$$\begin{aligned}\Phi_{pma} &= \hat{\Phi}_{pm}\cos(\frac{\pi}{\tau_p}x)\\ \Phi_{pmb} &= \hat{\Phi}_{pm}\cos(\frac{\pi}{\tau_p}x-\frac{2}{3}\pi)\\ \Phi_{pmc} &= \hat{\Phi}_{pm}\cos(\frac{\pi}{\tau_p}x-\frac{4}{3}\pi)\end{aligned} \tag{7}$$

where x is the translator position, which is zero in Fig. 3.

This flux follows a path different from the path followed by the flux caused by the translator currents and the reluctance is different from the air-gap reluctance. However, for our model, the flux in the translator teeth is of interest. Therefore, the magnetomotive force of the magnets is modelled as

$$\begin{aligned}F_{mpma} &= R_{mg}\Phi_{pma}\\ F_{mpmb} &= R_{mg}\Phi_{pmb}\\ F_{mpmc} &= R_{mg}\Phi_{pmc}\end{aligned} \tag{8}$$

In no-load, these magnetomotive forces result in the fluxes of (7), because saturation is negligible and therefore the tooth and yoke reluctances are negligible. When the teeth saturate, the fluxes caused by the magnets decrease, but the magnetomotive forces remain equal.

IV. Voltage Equations and Forces

A. Voltage equations

The voltages of the translator phases can be written as

$$\begin{aligned}u_a &= Ri_a+\frac{\mathrm{d}\lambda_a}{\mathrm{d}t} = Ri_a+N_t\frac{\mathrm{d}}{\mathrm{d}t}\left(\Phi_{a1}+\Phi_{a2}+\Phi_{a3}+\Phi_{a4}\right)\\ u_b &= Ri_b+\frac{\mathrm{d}\lambda_b}{\mathrm{d}t} = Ri_b+N_t\frac{\mathrm{d}}{\mathrm{d}t}\left(\Phi_{b1}+\Phi_{b2}+\Phi_{b3}+\Phi_{b4}\right)\\ u_c &= Ri_c+\frac{\mathrm{d}\lambda_c}{\mathrm{d}t} = Ri_c+N_t\frac{\mathrm{d}}{\mathrm{d}t}\left(\Phi_{c1}+\Phi_{c2}+\Phi_{c3}+\Phi_{c4}\right)\end{aligned} \tag{9}$$

where

R is the phase resistance,
i_a is the phase current of phase a,
λ_a is the flux linkage of phase a,
Φ_{an} is the flux in the n-th tooth of phase a, and
N_t is the number of turns around a tooth.

The no-load voltages are given by

$$\begin{aligned}e_{pa} &= -4N_t\frac{\pi}{\tau_p}\hat{\Phi}_{pm}\sin(\frac{\pi}{\tau_p}x)\frac{\mathrm{d}x}{\mathrm{d}t}\\ e_{pb} &= -4N_t\frac{\pi}{\tau_p}\hat{\Phi}_{pm}\sin(\frac{\pi}{\tau_p}x-\frac{2}{3}\pi)\frac{\mathrm{d}x}{\mathrm{d}t}\\ e_{pc} &= -4N_t\frac{\pi}{\tau_p}\hat{\Phi}_{pm}\sin(\frac{\pi}{\tau_p}x-\frac{4}{3}\pi)\frac{\mathrm{d}x}{\mathrm{d}t}\end{aligned} \tag{10}$$

Because some elements in the magnetic circuit are non-linear due to saturation, the equations for the fluxes have to be solved by means of an iteration process.

B. Force calculations

The power amplifier generates a three-phase current, which is made a function of the position:

$$\begin{aligned}i_a &= -\hat{i}\sin(\frac{\pi}{\tau_p}x+\varphi)\\ i_b &= -\hat{i}\sin(\frac{\pi}{\tau_p}x-\frac{2}{3}\pi+\varphi)\\ i_c &= -\hat{i}\sin(\frac{\pi}{\tau_p}x-\frac{4}{3}\pi+\varphi)\end{aligned} \tag{11}$$

where the current leads the no-load voltage with an angle φ, compare (10).

If the currents are so low that the teeth do not saturate, the electro magnetic force can be calculated from the no-load voltages and currents [18] as

$$F_{em} = 6\frac{\pi}{\tau_p}N_t\hat{\Phi}_{pm}\hat{i}\cos\varphi \tag{12}$$

Under saturated conditions, the electro magnetic force is calculated from the coenergy W_m' [14,18] as

$$F_{em} = \frac{\partial W_m'}{\partial x} \tag{13}$$

The coenergy is calculated [14,18] as

$$\begin{aligned}W_m'(i_a,i_b,i_c,x) = &\int_0^{i_a}\lambda_a(i_a',0,0,x)\mathrm{d}i_a' + \int_0^{i_b}\lambda_b(i_a,i_b',0,x)\mathrm{d}i_b'\\ &+\int_0^{i_c}\lambda_c(i_a,i_b,i_c',x)\mathrm{d}i_c' + W_{m0}'(x)\end{aligned} \tag{14}$$

where $W_{m0}'(x)$ is the coenergy when the currents are zero.

It is assumed that $W_{m0}'(x)$ is not a function of x. That this assumption is reasonable, appears from the fact that the cogging force is very small when the translator is moved over the magnets.

V. Calculated and Experimental Results

A. Force as a function of position and end effects

The force generated by the motor was measured as a function of the position x and the current amplitude $\hat{i}$, while the angle φ was kept zero. Current amplitudes up to 15 A were used, which is three times the rated continuous current.

Fig. 7 depicts the force calculated the magnetic circuit of Fig. 5 neglecting end effects. Fig. 8 depicts the force calculated with the magnetic circuit of Fig. 4 considering end effects. Fig. 9 depicts the measured force. Fig. 10 combines measurements and calculations. For current amplitudes up to about 7 A, the force increases linearly with the current, but at larger current amplitudes, the force increases less due to saturation.

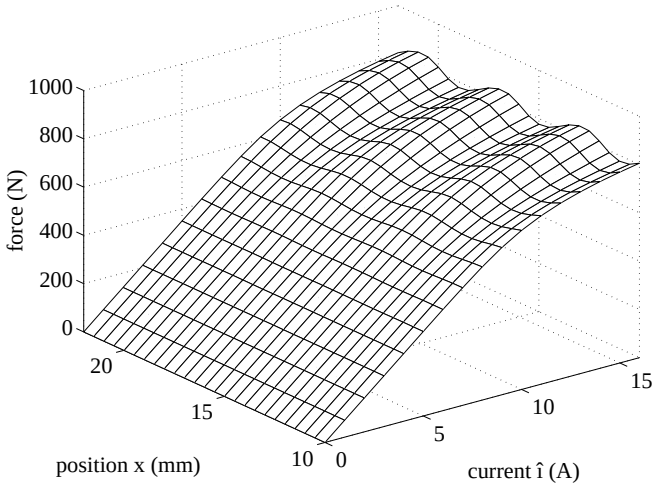

Fig. 7. Calculated force as a function of current amplitude and position neglecting end effects.

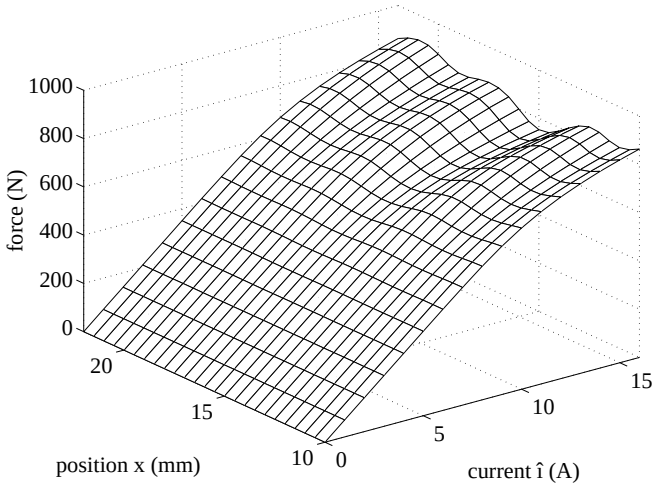

Fig. 8. Calculated force as a function of current amplitude and position considering end effects.

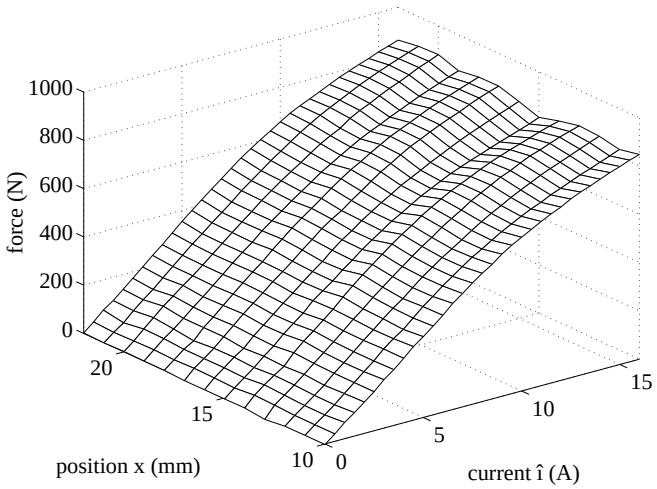

Fig. 9. Measured force as a function of current amplitude and position.

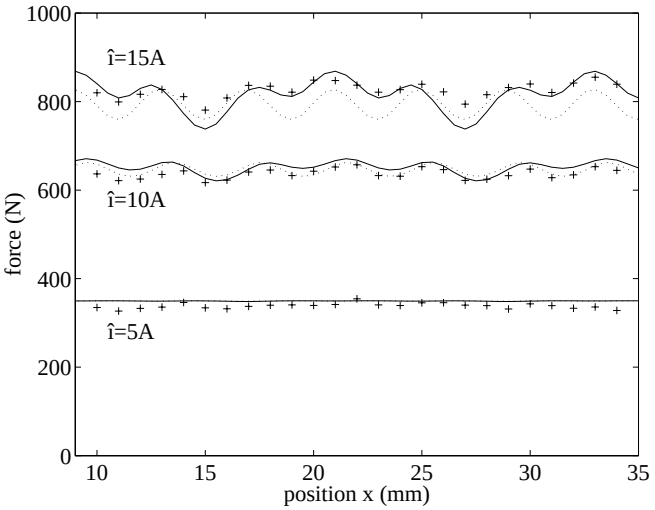

Fig. 10. Calculated force neglecting (..) and considering (-) end effects and measured (+) force as a function of position at three different current amplitudes.

If end effects are neglected, the force at high currents is periodic every 4 mm, because every 4 mm the same magnetic configuration comes back. If end effects are considered, an additional periodicity of the force arises every 12 mm, which is a pole pitch. In the measurements, both periodicities are present. It appears that the model including end effects exaggerates the periodicities, but the trends are clearly visible.

B. Maximum force to current ratio

For the force calculations in this section, the magnetic circuit of the motor neglecting end effects of Fig. 5 has been used.

The force generated by the motor was measured while the translator was kept in one position as a function of the current amplitude $\hat{i}$ and the angle φ, both introduced in (11).

Fig. 11 and Fig. 12 depict the force as a function of the angle φ for different current amplitudes in two different positions. For low current amplitudes, the force as a function of the phase angle is cosinusoidal, as expected from the linear model (12). However, for larger current amplitudes, the form of the force changes: the force is larger when the current leads the no-load voltage, especially in the position x=0.

To check the validity of this conclusion, Fig. 13 depicts the calculated force as a function of the current amplitude for two values of the angle φ at position x=0. The force generated with a current amplitude of 15 A at φ=15° is about 3% higher than the force generated with the same current at φ=0.

Fig. 14 and Fig. 15 depict the contour plot of the measured and the calculated force in the i_d-i_q plane in two different positions. Also the trajectory for maximum force to current ratio has been depicted. Again, the correlation between the trends of the calculated and measured contour plots of the force is rather good.

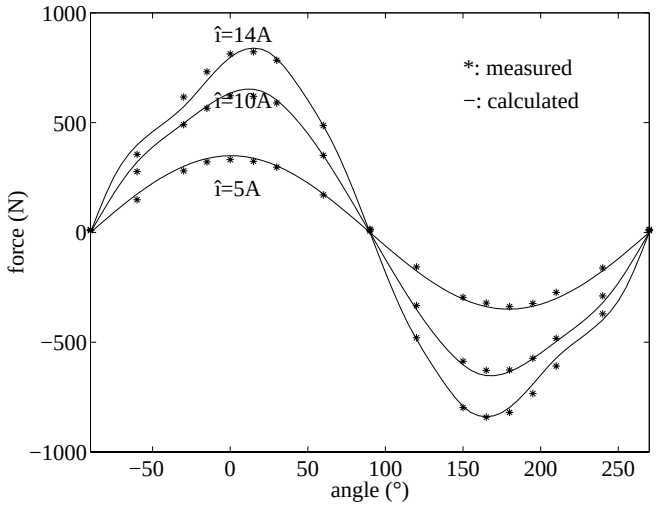

Fig. 11. Force as a function of angle at different current amplitudes in position x=0.

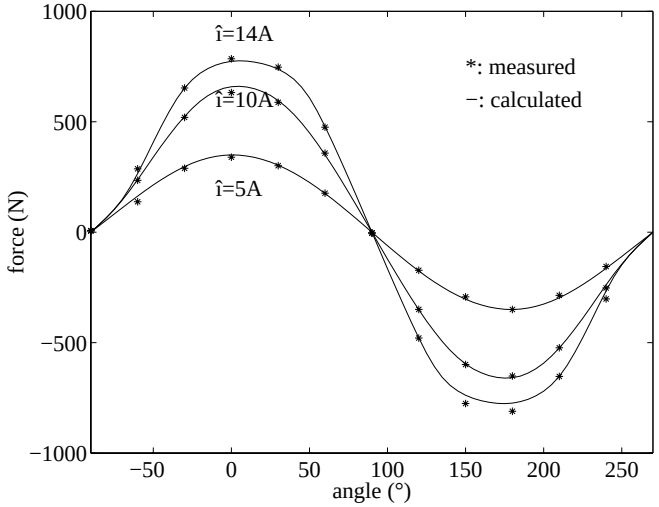

Fig. 12. Force as a function of angle at different current amplitudes in position x=2 mm.

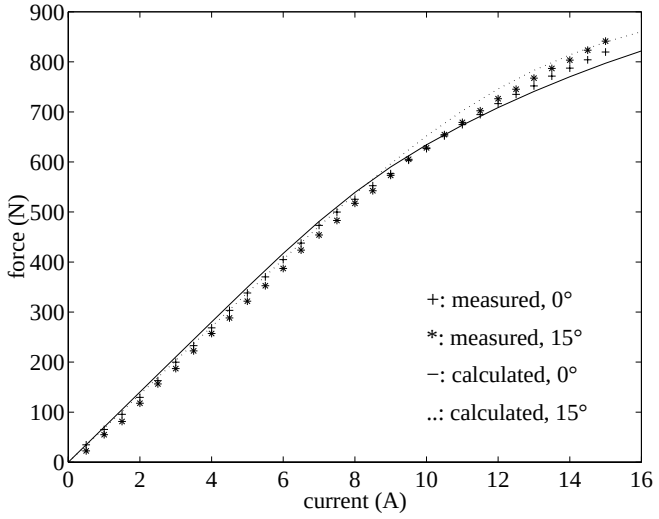

Fig. 13. Force as a function of current amplitude and angle at x=0.

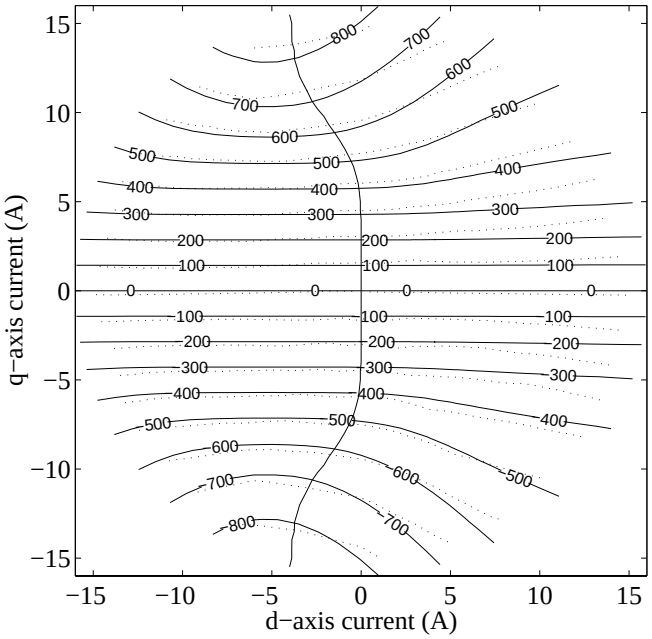

Fig. 14. Trajectory for maximum force to current ratio in a set of contour plots of the force in the i_d-i_q plane at position x=0, -: calculated, ..: measured.

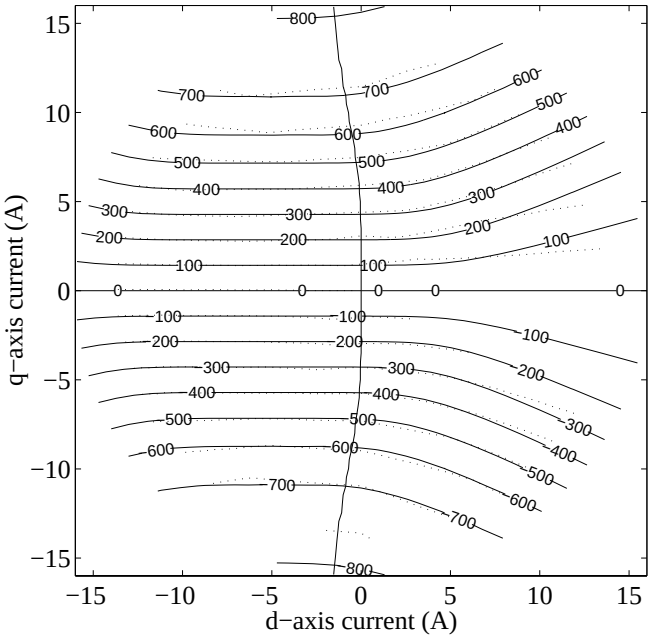

Fig. 15. Trajectory for maximum force to current ratio in a set of contour plots of the force in the i_d-i_q plane at position x= 2 mm, -: calculated, ..: measured.

In both positions, the maximum force to current ratio in saturation is obtained with a negative d-axis current. However, in position x=0, the optimum negative d-axis current is significantly larger than in position x=2 mm.

Fig. 16 depicts the calculated angle φ for maximum force to current ratio as a function of position and current amplitude.

The information of this picture can be incorporated in a control system. If this s too complicated, a strategy could be to work with a constant average angle φ of for example 10°.

It can be concluded that using a negative d-axis current increases the force in saturation. This effect can be explained from the fact that a negative d-axis current reduces the flux levels in the teeth, thus reducing the saturation level, while the q-axis current hardly decreases when the current amplitude remains constant.

The correlation between measurements and calculations is reasonable. Because of the rather rough magnetic circuit modelling, very accurate results can not be expected. However, both the measured and the calculated results confirm the conclusion that in a saturated machine, the force can be increased by using a negative d-axis current. Although this increase is not large, it is useful as well, because it results in a decrease in the terminal voltage, and therefore of the amplifier rating.

VI. Conclusions

This paper shows that it is possible to model a linear permanent-magnet motor including saturation using magnetic circuit theory. In saturated condition, the force becomes a function of the position, where end effects are not negligible. In saturation, a negative d-axis current results in an increase in the generated force, as appears from measurements as well as from calculations. Although the increase is not large, it is nevertheless useful, because a negative d-axis current also results in a decrease in the amplifier rating. The trajectory for maximum force to current ratio is different for different positions. The correlation between the calculated and the measured force justifies the model.

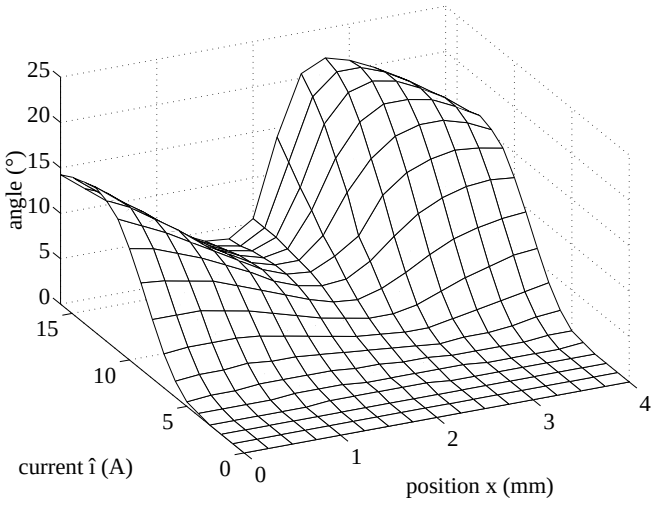

Fig. 16. Angle φ for maximum force to current ratio as a function of position and current.

Acknowledgement

The authors want to thank Mr A.T.A. Peijnenburg, Philips CFT, Eindhoven, for providing them with the linear PM motor for the experimental work.

References

[1] J.F. Gieras and Z.J. Piech, *Linear synchronous motors: transportation and automation systems*, Boca Raton: CRC Press, 2000.

[2] S.A. Nasar, I. Boldea and L.E. Unnewehr, *Permanent magnet, reluctance and self-synchronous motors*, Boca Raton: CRC Press, 1993.

[3] N. Mohan, *Electric drives, an integrative approach*, NMPERE, Minneapolis, 2001.

[4] M. Sanada., S. Morimoto and Y. Takeda, "Interior permanent magnet linear synchronous motor for high-performance drives", in *IEEE transactions on industry applications*, 1997, vol. 33, pp. 966-972.

[5] C. Mademlis and V.G. Agelidis, "On considering magnetic saturation with maximum torque to current control in interior permanent magnet synchronous motor drives", in *IEEE transactions on energy conversion*, 2001, vol. 16, pp. 246-252.

[6] G. Hong, X. Qiang and J. Zhenchun, "Effects and compensation of magnetic saturation in flux-weakening controlled interior permanent magnet linear synchronous motor", in *Proceedings of the Fifth International Conference on Electrical Machines and Systems*, Beijing, China, 2001, vol. 2, pp. 913-916.

[7] B.J. Chalmers., L. Museba and D.F. Gosden, "Variable-frequency synchronous motor drives for electric vehicles", in *IEEE transactions on industry applications*, 1996, vol. 32, pp. 896-903.

[8] N. Bianchi and S. Bolognani, "Parameters and volt-ampere ratings of synchronous motor drive for flux-weakening applications", in *IEEE transactions on power electronics*, 1997, vol. 12, pp. 895-903.

[9] S. Morimoto, Y. Takeda, T. Hirasa and K. Taniguchi, "Expansion of operating limits for permanent magnet motor by current vector control considering inverter capacity", in *IEEE transactions on industry applications*, 1990, vol. 26, pp. 866-871.

[10] S. Morimoto., M. Sanada and Y. Takeda, "Loss minimization control of permanent magnet synchronous motor drives", in *IEEE transactions on industrial electronics*, 1994, vol. 41, pp 511-517.

[11] R.S. Colby and D.W. Novotny, "Efficient operation of surface-mounted PM synchronous motors", in *IEEE transactions on industry applications*, 1987, vol. 23, pp. 1048-1054.

[12] M. Platen, G. Henneberger, 'Examination of leakage and end effects in a linear synchronous motor for vertical transportation by means of finite element computation', in *IEEE Transactions on Magnetics*, 2001, vol.37, pp.3640-3643.

[13] V. Ostovic, J.M. Miller, V.K. Grag, R.D. Schultz and S.H. Swales, "A magnetic-equivalent-circuit-based performance computation of a Lundell alternator", in *IEEE transactions on industry applications*, 1999, vol. 35, pp. 825-830.

[14] H. Polinder, J.G. Slootweg, J.C. Compter and M.J. Hoeijmakers, "Modelling a linear PM motor including magnetic saturation", in *Proceedings of the IEE International Conference on Power Electronics, Machines and Drives*, Bath, April 2002, pp. 632-637.

[15] W. Lenders, "The orthocyclic method of coil winding", in *Philips technical review*, 1961/1962, vol. 23, pp. 365-404.

[16] R. Richter, *Elektrische Maschinen, erster Band*, third edition, Basel: Birkhäuser, 1967.

[17] J. Jansen, *Materials Library*, third edition, Philips Report CTR505-90-RJ261, Eindhoven, 1990.

[18] A.E. Fitzgerald, C. Kingsley and S.D. Umans, *Electric machinery*, Sixth edition, London: McGraw-Hill, 2002.